A comparison study of experimental and direct numerical simulation results associated with dynamics and heat transfer of a boiling bubble

Satbyoul Jung [a], Yasuo Ose [b], Hyungdae Kim [a*], Tomoaki Kunugi [c]
[a]*Department of Nuclear Engineering, KyungHee Univ., Republic of Korea*
[b]*Yamato System Engineer Co., Ltd., Japan*
[c]*Deparment of Nuclear Engineering, Kyoto Univ., Japan*

[*]*Corresponding author: hdkims@khu.ac.kr*

1. Introduction

Nucleate boiling is widely used in industries due to very high heat transfer efficiency. Thus, its physical mechanisms have been extensively explored over the last few decades. Recently, a number of boiling simulations coupling with various interface tracking methods have been performed for the accurate modelling to predict actual characteristics and mechanisms of boiling heat transfer [1-3]. However, there is a lack in high-quality experimental data to validate the simulation results with interface tracking for nucleate boiling heat transfer.

In the present study, a systematic comparison between the state-of-the-art experimental measurements and numerical simulations is tried with focus on liquid-vapor phase and heat transfer distributions on the heater surface during nucleate boiling of a single bubble. In the experiment, by applying both a total reflection technique which consisted of a coherent laser and an infrared thermometry to a boiling surface with high spatial and temporal resolution, the liquid-vapor phase and the heat transfer distributions underneath a growing bubble were simultaneously measured. In the simulation, nucleate boiling process of a single bubble was simulated by using the MARS (Multi-interface Advection and Reconstruction Solver) including a non-empirical boiling and condensation model.

2. Experiment

2.1 Experimental technique

An unique experimental method is introduced to temporally synchronize and spatially map surface temperature distribution using infrared thermometry [4,5], liquid–vapor phase distribution using total reflection technique [6,7], and the microlayer geometry using laser interferometry [8,9], of a boiling surface during single-bubble nucleate boiling. The present experimental method integrating the three different optical techniques provides unique high-quality experimental measurement data of hydrodynamic and thermal characteristics associated with a boiling bubble growing on a heated surface.

The total reflection technique permits to visualize the distribution of liquid and vapor phases on the surface. Total reflection occurred for the vapor phase, but not for the liquid phase, so that the resulting images appeared bright in the dry areas and dark in the wet areas. An incoherent light source is generally used for conventional total reflection. When a coherent source (i.e., a laser) is used for total reflection, interference patterns appear due to the microlayer beneath the boiling bubble.

The history of local temperature distributions of a boiling surface measured by infrared thermometry technique is used as the boundary conditions to numerically calculate the transient heat conduction of the heater plate. As a result, a three-dimensional temperature profile of the heater plate was obtained for each time step, and the surface heat flux was calculated based on the temperature gradient normal to the boiling surface.

We used a combination of an ITO thin-film heater, transparent to visible light and opaque to infrared light, and a calcium fluoride (CaF_2) plate, transparent to both visible and infrared light, to spatially and temporally synchronize the surface temperature distribution using infrared thermometry, the liquid–vapor phase distribution using a total reflection technique, and the microlayer geometry using laser interferometry during nucleate boiling.

2.2 Experimental setup and conditions

A high-speed camera and a HeNe laser were used for the simultaneous total reflection and laser interferometry measurements. Another high-speed camera was installed to visualize the dynamics of the boiling bubble from the side. A high-speed infrared camera was used to measure the temperature distribution on the boiling surface at the center of the substrate where the prism blocks were not installed. Further details of experimental setup is in [10-12].

The experiment data were obtained for single-bubble nucleate boiling of water at ΔT_{sub} = 3℃ and q''_{avg} = 53 kW/m^2 under atmospheric pressure. The spatial and temporal resolutions were 17 μm and 0.083 ms for the side image, 32 μm and 0.083 ms for the phase detection

and 84 μm and 0.83 ms for the heat transfer measurement, respectively.

3. Numerical Simulation

The unsteady two-dimensional numerical simulations based on the MARS [13] coupled with the non-empirical boiling and condensation model were performed for a single bubble nucleate boiling from a heated surface.

3.1 Governing equations

The governing equations of the MARS are consisted of the continuity equation for multi-phase flow, the momentum equation based on a one-fluid model and the energy equation as follows:

$$\frac{\partial F_m}{\partial t} + \nabla(F_m u) - F_m \nabla u = 0 \quad (1)$$

$$\frac{\partial u}{\partial t} + \nabla \cdot (uu) = G - \frac{1}{\langle \rho \rangle} \nabla P - \nabla \cdot \tau + \frac{1}{\langle \rho \rangle} F_v \quad (2)$$

$$\frac{\partial}{\partial t} \langle \rho C_v \rangle T + \nabla \cdot (\langle \rho C_v \rangle T u) = \nabla(\langle \lambda \rangle \nabla T) - P(\nabla \cdot u) + Q \quad (3)$$

where F is volume of fluid (VOF) fraction, the subscript m denotes the *m*-th fluid or phase, u is velocity, t is time, P is pressure, T is temperature, G is gravity, is viscous shear stress, F_v is body force due to surface tension based on the continuum surface force model [14], ρ is density, C_v is specific heat at constant volume, λ is thermal conductivity, Q is heat source and bracket denotes an average of thermal properties. In order to satisfy the conservation of F, the third term of the continuity equation must be included. The second term of the right hand side of the energy equation, Eq. (4), i.e., the Clausius-Clapeyron relation was considered as the external work done by the phase change, e.g., a bubble oscillation caused by the expansion and contraction with the bubble growth and condensation processes. The interface volume-tracking technique [13] was applied to the second term of the continuity equation in the MARS. The projection method [15] was applied to solve the momentum equation and the pressure Poisson equation was solved by the Bi-CGSTAB [16].

3.2 Non-empirical boiling and condensation model

The boiling and condensation model in the MARS for the subcooled nucleate boiling phenomena consisted of both a nucleation model and a bubble growth-condensation model [17]. The bubble growth-condensation model is based on the temperature-recovery method [18]. This model was applied only to the interfacial cells which have the VOF fraction between 0 and 1. The original temperature-recovery model could not treat a large volume change in the expansion and condensation processes because the temperature-recovery method was originally developed for the solidification/melting of metals not for the water-vapor phase-change system. Therefore, a density-change between water and vapor was considered as a volume-change by a phase-change ratio, Δg_v, as expressed as:

$$\Delta g_v = \left(\rho_l Cp_l \Delta T\right) \Big/ \left(\rho g h_{lv}\right) \quad (5)$$

where Cp_l is specific heat at constant pressure, ΔT is degree of superheat or subcooling, h_{lv} is latent heat and the subscript *g* and *l* denote gas and liquid phases, respectively. Eq. (5) represents that the ratio of the sensible heat to the latent heat at the interfacial cell. In order to satisfy the conservation of the volume, the following constraint condition must be satisfied:

$$\left(F_l - \left|\Delta g_v\right|\right) + \left(F_l + \left|\Delta g_v\right|\right) = 1 \text{: At evaporation} \quad (6)$$

$$\left(F_l + \left|\Delta g_v\right|\right) + \left(F_l - \left|\Delta g_v\right|\right) = 1 \text{: At condensation} \quad (7)$$

Moreover, the original bubble growth-condensation model was based on the assumptions of both a zero-thickness interface and a "rapid" change of "State 1 (Water)" to "State 2 (Vapor)" or vice versa based on the quasi-thermal equilibrium hypothesis. However in this model, a "very slow" change of "State 1" to "State 2" in the quasi-thermal equilibrium hypothesis was ignored. In the real system, the finite thickness of interface exists and both "very slow" and "rapid" changes simultaneously occur in the phase-change process. In order to consider a relaxation or waiting time for consuming the latent heat at the interface region in the phase-change process, the unsteady heat conduction in the finite interface region as the "very slow" change process was considered as follows: The relaxation time $\Delta\tau$ can be considered that the phase-change front passes through the fictitious interface thickness Δ, so that $\Delta\tau$ can be defined by using the thermal diffusivity of the water as follows:

$$\Delta\tau = \Delta^2 / \alpha \quad (8)$$

On the other hand, a thermal penetration length δ for the unsteady heat conduction in a semi-infinite slab with a constant boundary temperature was approximated by the following expression:

$$\delta = \sqrt{12\alpha t} \quad (9)$$

If the thermal penetration depth can be considered as the same as the fictitious interface thickness, $\Delta\tau$ can substitute into t of Eq. (9): $\delta = \sqrt{12}\Delta$. As the result, an

invariant relation between the thermal penetration length and the fictitious interface thickness can be obtained as follows:

$$\Delta / \delta = (\sqrt{12})^{-1} \approx 0.3 \quad (10)$$

Therefore, the rapid phase-changed volume during $\Delta\tau$ will be 70% of the thermal penetration depth, not 100%. This corresponds to the "very slow" change and can be occurred in 30% of the thermal penetration depth, i.e., the computational interface thickness. In this study, the relaxation time can be considered if a VOF limiter is introduced as a phase-change denominator or limiter. For example, the relaxation time for both phase fronts is assumed to be 15% at both interfaces of evaporation and condensation:

$$\text{VOF limiter} : 0.15 \le F \le 0.85 \quad (11)$$

3.3 Computational domain

The computational domain size was 12 mm ×10 mm. The grid size was 60 μm in x- and z- directions, respectively and time step in the computation was set to 10 μs. The boundary conditions on both sides (±x), bottom (-z) and top (+z) of computational domain were periodic, non-slip wall, free-flow (zero pressure gradient) conditions, respectively. The computational conditions were basically the same as the experiments. Initial pressure was set to an atmospheric pressure and three subcooling conditions of water were investigated (0.1, 1.0, 2.0, 3.0℃). The thin-film electric heater used in the experiment was located on the CaF_2 base plate, which supply the input heat flux of 53 kW/m^2 and the initial surface temperature of 122℃ which was from the experimental conditions. The static contact angle between the liquid and surface was taken to be 15° less than that of experiment, for which the effect of dynamic contact angle was not considered in this simulation. The initial bubble temperature was also set to the saturated temperature corresponding to an atmospheric pressure. The initial temperature field in this computations was assumed to be gradient by the conduction from wall to liquid during the waiting time obtained from the experimental data and the initial velocity field was stationary.

3.4 Numerical simulation results for a single bubble

The visualization result obtained from numerical simulation for single-bubble nucleate boiling of water in subcooling of 0.1 ℃ is presented in Fig. 1, showing the liquid-vapor interface and temperature distribution in computational domain during a cycle of bubble growth. The data of liquid-vapor interface tracking enables to observe the dynamics of liquid-vapor-solid triple contact line as well as liquid-vapor interface. From the data of temperature distribution nearby the heated surface, the surface temperature, T_s and the surface heat flux, q_w can be defined as follows:

$$q_w = \lambda_f \frac{T_s - T_f}{\Delta x_s} \quad (12)$$

$$T_s = \frac{\lambda_f T_f \Delta x_{s,f} + \lambda_w T_w \Delta x_{s,w}}{\lambda_f \Delta x_{s,f} + \lambda_w \Delta x_{s,w}} \quad (13)$$

where Δx_s is distance from the cell to the heated surface. The subscripts *f* and *w* denote the fluid and wall computational cells adjacent to the heating surface, respectively.

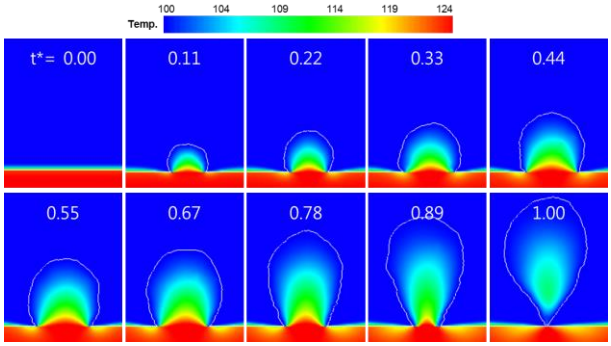

Fig. 1. Numerical simulation results for liquid-vapor interface and temperature distribution in computational domain (ΔT_{sub} = 0.1℃, q''_{avg} = 53 kW/m^2).

3. Results and Discussion

We determined a set of experimental and computational results for a systematic comparison between the experimental measurements and numerical simulations with focus on liquid-vapor phase and heat transfer distributions on the heater surface during nucleate boiling of a single bubble. The initial surface temperature and input heat flux in the simulation were set to be same as those in the experiment, 122℃ and 53 kW/m^2. However, liquid subcooling was different, 3℃ in experiment versus 0.1℃ in numerical simulation. In addition, instead of the comparison with time, the dimensionless time-evolution normalized to the bubble departure time, t_D, of dimensionless bubble radius normalized to the bubble departure radius, r_D, was plotted in Fig. 2. It is supposed that the difference of liquid subcooling and bubble growth time resulted from the two-dimensionality effect and the thickness of superheated layer and the initial fluid motion which can be unmeasured by the experiment.

We present the comparison of experiment (ΔT_{sub} = 3.0℃) and numerical simulation (ΔT_{sub} = 0.1℃) results with the dimensionless time normalized to bubble departure time and attempt the qualitative analysis with them as a feasibility study.

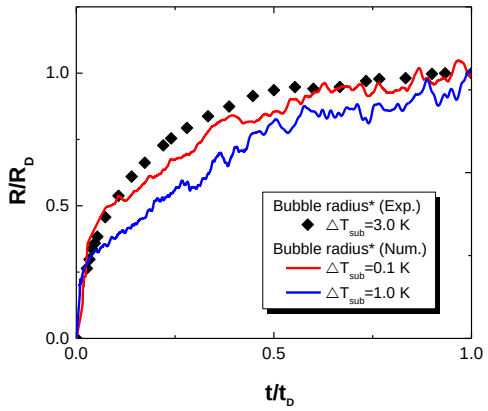

Fig. 2. Comparison of dimensionless time-evolution of dimensionless bubble radius between experiment and numerical simulation results.

4.1 Comparison of liquid-vapor phase and the heat transfer distributions between experimental and numerical results

The data with focus on the physical interpretation and qualitative analysis for some inconsistency between the experiment and numerical simulation is investigated. From them for single bubble, the temperature and heat flux distributions on the heated surface and temperature in the heater with changing the bubble geometry for each time step are shown in Fig. 3.

There are four steps with time, before the bubble nucleation, during the bubble growth period and the bubble detachment period, and the bubble rising.

Before the bubble nucleates, the superheat of boiling surface is uniform in the range from 121 to 123℃. The surface heat flux is quite uniform in both the experiment and numerical simulation results, but the magnitude of surface heat flux seems to be a bit different. Compared to the average heat flux (53 kW/m^2) in the experiment, the surface heat flux in numerical simulation is slightly higher (see t*=0 in Fig. 3). However, it is not strange as the difference within the uncertainty of the heat flux measurement, 100 kW/m^2.

In the beginning of bubble growth, the bubble grows rapidly and the wall heat transfer responded it. There were differences in both macroscopic bubble dynamics and microscopic thermal characteristics between the experimental and numerical simulation results.

In terms of macroscopic bubble dynamics, it is observed that the bubble growth in the experiment is faster than that in the numerical simulation and that the bubble shape is spherical in the experiment and hemispherical in the numerical simulation. It is supposed that this inconsistency was resulted from the difference in temperature of the superheated liquid layer thickness surrounding the boiling bubble. In addition, the contact angle for boiling process changes dynamically between advancing and receding contact angles, but the effect of dynamic contact angle was not included in this simulation which would clearly affect the macroscopic bubble dynamics.

With regard to the microscopic thermal characteristics of the boiling surface, in the experimental result, the significant heat flux (~1.0 MW/m^2) is observed in the relatively wide area of the bubble base where the extended microlayer exists (t*=0.39). Such a high heat flux due to microlayer evaporation results in a considerable drop of local surface temperature. In the numerical simulation result, the relatively small amount of heat flux (~0.3 MW/m^2) is observed only near the triple contact line of the bubble base without the extended microlayer and the local drop in surface temperature appears. In addition, surface temperature of the dry region inside the triple contact line gradually increases due to the zero surface heat flux. The effect of microlayer beneath a boiling bubble was not included in this simulation because it for microlayer with a few microns in thickness requires tremendously small grid size with nano-scale and huge computational cost. Therefore, the local surface temperature at the dry region continuously increases without cooling in the simulation. In the experimental observation, however, the high heat flux resulted from the microlayer evaporation appears and continues until depletion of the microlayer (t*=0.67), which effectively delays local overheating of the bubble base. These effects during the bubble growth period influenced to the characteristics of heat transfer during the bubble detachment period.

It seems that the microlayer evaporation is an effective heat transfer removal mechanism, but however was found that the contribution of microlayer evaporation to the total heat flow rate for the bubble growth was estimated to be less than 17% in the previous studies [10-12]. It indicates that microlayer evaporation is not a dominant heat transfer mechanism in interpreting the growth history of a boiling bubble. This is consistent with previous estimates [19, 20].

The bubble in experiment started to detach after the microlayer was depleted (t*=0.67) and the bubble in simulation started to detach at the same dimensionless time. During the detachment period, the bubble base shrank and the triple contact line receded. The heat flux distribution had a small peak near the receding contact line (~0.2 MW/m^2). It shows a good agreement with numerical simulation results in an order of magnitude of heat flux near the triple contact line.

There are further more detailed observations of heat transfer distribution for both experiment and numerical simulation during the detachment period. While the magnitude of heat flux gradually decrease after the microlayer depletion in experimental results, that of numerical simulation slightly increase as the triple contact line receded. As the results, there is difference of the magnitude of heat flux. When the bubble base shrinks, the cold bulk liquid quenched the area of the bubble influence, leading to the heat transfer by

quenching, as well as heat transfer by evaporation near the triple contact line. The temperature difference between the dry region and cold bulk liquid causes the heat transfer by quenching. When the bubble started to shrink (t*=0.67), the local temperature in dry region reached to 124℃ in the numerical simulation, whereas that in the experiment is less than 120℃ due to the cooling by the evaporation. It results in more quenching heat flux near the triple contact line in the numerical simulation rather than the experiment.

After the bubble was detached from the heated wall, the heat fluxes of 0.1 and 0.3 MW/m^2 at the bubble center in both the experimental and numerical simulation results respectively, occurred due to the wake flow by rising bubble.

4. Conclusions

The experimental measurement and numerical simulation data of a boiling bubble on a heated wall were presented and compared in detail with focus on liquid-vapor phase and heat transfer distributions on the boiling surface. In the experiment, the technique is based on spatial and temporal synchronization of an infrared thermometry technique for the local heat transfer measurement, a total reflection technique for the liquid-vapor phase detection, and a laser interferometry technique for detection of the microlayer geometry. In the simulation, a single bubble nucleate boiling was simulated by using the MARS including a non-empirical boiling and condensation model. The major findings from the present comparison study are following:

- The microlayer evaporation could affect the characteristics of heat transfer for a bubble growth cycle. At the beginning of bubble growth, the effective heat transfer from a heated wall occurs due to microlayer evaporation, which impeded the local wall superheated in the dry region.
- During the bubble detachment period, the heat flux by evaporation and quenching of cooling liquid near triple contact line could be observed. It showed a good agreement between numerical simulation and experimental results in an order of magnitude of heat flux.

In addition, it is supposed from this study that the thermal boundary layer thickness and velocity distribution just before a bubble nucleates play a key role in determining bubble growth rate and departure behavior. Therefore, ad-hoc experiments to obtain the velocity and temperature field before a bubble nucleation, such as using PIV (particle image velocimetry) and LIF (laser induced fluorescence) techniques, are ongoing in our laboratory

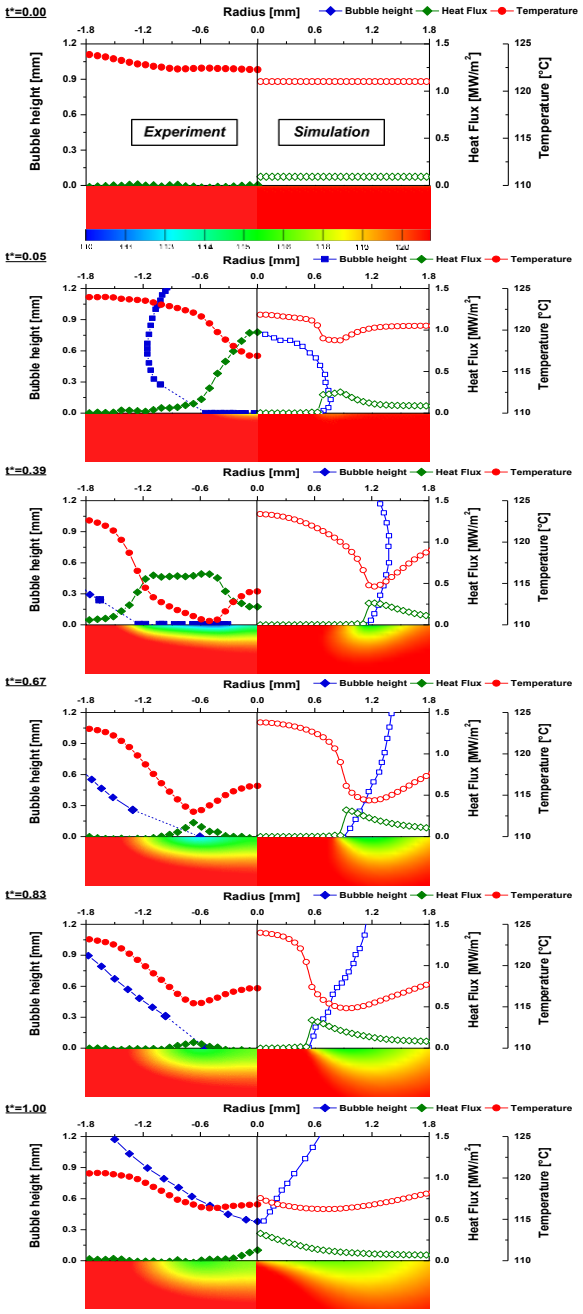

Fig. 3. Comparison of liquid-vapor phase and heat transfer distributions on the heater surface during nucleate boiling of a single bubble between experiment and numerical simulation results.

REFERENCES

[1] Son. G., Dhir V. K., Dynamics and heat transfer associated with a single bubble during nucleate boiling on a horizontal surface, Journal of Heat Transfer, Vol. 121, p. 623-631, 1999.

[2] Kunkelmann C., Ibrahem. K., Schweizer. N., Herbert S., Stephan. P., Gambaryan-Rosiman. T., The effect of three-phase contact line speed on local evaporative heat transfer: Experimental and numerical investigations, Int. J of Heat and Mass Transfer, Vol. 55, p. 1896-1904, 2012.

[3] Ose. Y., Kunugi. T., Numerical study on bubble hevaiour and heat transfer characteristics of subcooled pool boiling

based on non-empirical boiling and condensation model, Proc. of 8th Int. Conference on Multiphase Flow, ICMF2013-699, p. 1-8, 2013.
[4] Theofanous. T. G., Dinh. T. N., High heat flux boiling and burnout as microphysical phenomena: mounting evidence and opportunities, Multiphase Science and Technology, Vol. 18, p. 251-276, 2006.
[5] Gerardi. C., Buongiorno. J., Hu. L. W., McKrell. T., Study of bubble growth in water pool boiling through synchronized, infrared thermometry and high-speed video, Int. J. Heat Mass Transfer, Vol. 53, p. 4185-4192, 2010.
[6] Nishio. S., Gotoh. T., Nagai. N., Observation of boiling structures in high heat-flux boiling, Int. J. Heat and Mass Transfer, Vol. 41, p. 3191-3201, 1998.
[7] Chu. I. C., No. H. C., Song. C. H., Visualization of boiling structure and critical heat flux phenomenon for a narrow heating surface in a horizontal pool of saturated water, Int. J. Heat and Mass Transfer, Vol. 62, p. 142-152, 2013.
[8] Jawurek. H. H., Simultaneous determination of microlayer geometry and bubble growth in nucleate boiling, Int. J. Heat Mass Transfer, Vol. 12, p. 843-846, 1969.
[9] Koffman, L. D., Plesset. M. S., Experimental observations of the microlayer in vapor bubble growth on a heated solid, Journal of Heat Transfer, Vol. 105, p. 625-632, 1983.
[10] Jung. S., Kim. H., Synchronized measurement of liquid-vapor phase and temperature distributions on a boiling surface during single bubble nucleate boiling, Proc. of 8th Int. Conference on Multiphase Flow, ICMF2013-528, p. 1-10, 2013.
[11] Jung. S., Kim. H., An experimental method to simultaneously measure the dynamics and heat transfer associated with a single bubble during nucleate boiling on a horizontal surface, Int. J. Heat and Mass Transfer, Vol. 73, p. 365-375, 2014
[12] Jung. S, Kim. H, Simultaneous investigation of dynamics and heat transfer associated with a single bubble nucleate boiling, Transactions of the Korean Nuclear Society Autumn Meeting, 2013
[13] Kunugi. T., MARS for multiphase calculation, Computational Fluid Dynamics Journal, 9, p. 563-571, (2001).
[14] Brackbill. J. U., Koth. D. B., Zemach. C., A continuum method for modeling surface tension, Journal of Computational Physics, Vol. 100, p. 335-354, 1992.
[15] Chorin. A., Numerical solution of the Navier-Stokes equations. Mathematics of Computation, 22, p. 754-762, 1968.
[16] Van Der Vorst. H. A., BI-CGSTAB: A fast and smoothly converging variant of BI-CG for the solution of nonsymmetric linear system, SIAM Journal of Scientific and Statistical Computing, Vol. 13, p. 631-644, 1992.
[17] Kunugi. T., Saito. N., Fujita. T., Serizawa. A., Direct numerical simulation of pool and forced convective flow boiling phenomena, Proc. 12th International Heat Transfer Conference, 2002.
[18] Ohnaka. I., Introduction to computational analysis of heat transfer and solidification –application to the casting processes-, Maruzen, 202, 1985. (in Japanese)
[19] Myers. J. G., Yerramilli. V. K., Hussey. S. W., Yee. G. F., Kim. J., Time and space resolved wall temperature and heat flux measurements during nucleate boiling with constant heat flux boundary condition, Vol. 35, p. 73-86, 1992.
[20] Chu. I. C., Application to visualization techniques to the boiling structures of subcooled boiling flow and critical heat flux, Ph.D. Thesis, Korea Advanced Institute of Science and Technology, 2011.